Fabrication of hyperbranched polyamine functionalized graphene for high-efficiency removal of Pb(II) and methylene blue

Lihua Hu[a], Zhongping Yang[a], Limei Cui[b], Yan Li[a], Huu Hao Ngo[c], Yaoguang Wang[a], Qin Wei[a], Hongmin Ma[a], Liangguo Yan[b], Bin Du[b]

[a] Key Laboratory of Chemical Sensing & Analysis in Universities of Shandong, School of Chemistry and Chemical Engineering, University of Jinan, Jinan 250022, China
[b] School of Resources and Environment, University of Jinan, Jinan 250022, China
[c] School of Civil and Environmental Engineering, University of Technology Sydney, Broadway, NSW 2007, Australia

Highlights

- HPA-GO was firstly prepared for Pb(II) and methylene blue removal.
- The pseudo-second-order model and Langmuir model fitted the adsorption process.
- The thermodynamics implied the adsorption was endothermic and spontaneous.
- The adsorption mechanisms were discussed.
- HPA-GO could be recycled efficiently in the adsorption–desorption cycles.

Abstract

Multifunctional hyperbranched polyamine modified graphene oxide (HPA-GO) was successfully prepared and characterized by Fourier transform infrared spectroscopy (FTIR), thermogravimetric analysis (TGA), X-ray diffraction (XRD), zeta potential and scanning electron microscope (SEM) analyses. HPA-GO exhibited excellent adsorption performance for the removal of a heavy metal (Pb(II)) and a dye (methylene blue (MB)). The equilibrium adsorption capacity was 819.7 mg g^{-1} for Pb(II) and 740.7 mg g^{-1} for MB under the optimal conditions. The pseudo-second order equation and the Langmuir model exhibited good correlation with the adsorption kinetic and isotherm data, respectively, for these two pollutants. The thermodynamic results ($\Delta G < 0$, $\Delta H > 0$, $\Delta S > 0$) implied that the adsorption process of Pb(II) and MB was feasible, endothermic and spontaneous in nature. A possible adsorption mechanism has been proposed where chelation and electrostatic attraction dominated the adsorption of Pb(II) and π–π stacking interactions and electrostatic attraction dominated the adsorption of MB. In addition, the excellent reproducibility endowed HPA-GO with the potential for application in water treatment.

Keywords: Adsorption; Pb(II); Methylene blue; Kinetics and isotherm; Reproducibility

1. Introduction

Industrial development has resulted in increased environment pollution. Therefore, the decontamination of wastewater containing heavy metal ions and synthetic dyes from mining, metallurgical and dye manufacturing processes has become an urgent issue in the field of environment treatment [1]. Heavy metals and dyes are two of the most basic pollutants in wastewater due to their strong toxicity, non-biodegradability and accumulation in plants, animals and human beings [2] and [3]. Heavy metal ions, such as lead, can cause sickness, neurological disorders, kidney disease, anemia and even death [2]. The plastics, leather, papermaking and textile industries are some common sources of dye effluents. Dyes with a complex aromatic structure are more stable and difficult to biodegrade. Methylene blue (MB), which is the most commonly used substance for dying cotton, wood or silk, may cause nausea, vomiting and neurological injury in humans after frequent contact [3]. Due to their enormous harmful effects, heavy metals and synthetic dyes should be removed from wastewater prior to being released into the environment. Traditional technologies that have been explored for the removal of these contaminants include chemical precipitation, membrane filtration, adsorption, biological treatment, conventional coagulation and photocatalytic degradation [4] and [5]. Among these methods, adsorption is regarded as the most effective and widely used approach due to its relatively low cost, simple operation, and availability for many pollutants [6]. Therefore, various adsorbents, such as activated carbon [7], zeolite [8], clay [9] and polymeric adsorbents [10], have been produced to meet different needs. However, these traditional adsorbents are typically limited by low adsorption capacities or recycling problems. Therefore, the development of new adsorbents with better adsorption performance is highly desirable.

Recently, nanostructured adsorbents have been widely explored due to their high specific surface areas and enhanced active sites. As an emerging carbon nanomaterial, graphene has attracted considerable attention due to its unique properties. Due to its very large surface area, flat structure and good mechanical properties, graphene has been used as an excellent adsorbent to remove a range of heavy metals and benzenoid contaminants [11] and [12]. However, the performance of graphene nanoadsorbents is limited by the relatively low density of surface functional groups and poor water dispersibility caused by aggregation via van der Waals interactions [13]. To improve dispersion properties in aqueous solutions as well as the adsorption capacity, graphene is often functionalized with inorganic nanoparticles, surfactants, hydrophilic groups, or polymers [14] and [15].

Polymer adsorbents, such as polypyrrole [16], polythioamides [17], polyacrylamide [18], polyacrylic acid [19] and chitosan [20], are effective for removing heavy metals and dyes. Therefore, water-soluble polymers containing heteroatoms (N, O, S, P) are typically chosen to modify graphene oxide (GO) and generate polymer/GO nanosorbents. This modified procedure endows polymer/GO with good water solubility and abundant functional groups, which is beneficial for improving its adsorption capacity [21]. Wang et al. [22] dotted polyaniline nanorods on graphene oxide nanosheets to prepare a novel super adsorbent with a superb removal capacity for Cr(VI). Liu et al. [23] successfully prepared water-soluble cyclodextrin/poly(acrylic acid)/graphene oxide nanocomposites as new adsorbents for the removal of cationic dyes from aqueous solutions. Wang et al.[24] fabricated a series of polydopamine layer coated GO (PD/GO) composites, which were used for the removal of organic dyes and heavy metal ions with a very high capacity.

In comparison to linear polymers, hyperbranched polymers (HPs) are more suitable for the modification of GO to prepare an adsorbent due to its nearly spherical structure and numerous surface functional groups. In addition, most of the functional groups can interact with adsorbates due to weak or even non-existent molecular chain entanglements that exist in HP [25]. HP has been used to modify some substrates, such as SiO_2[26], fibers [27] and membranes [28], for the effective removal of heavy metals and dyes. However, no studies have employed hyperbranched polyamine modified GO as an adsorbent.

In this study, we combined multifunctional hyperbranched polyamine (HPA) with high surface area GO to prepare a novel nanosorbent (HPA-GO) for the high efficiency removal of both heavy metals and dye. Due to the abundant hydroxyl and amine groups, HPA exhibited good water solubility and strong affinity for the pollutants. Grafting of HPA onto the GO surface is expected to effectively improve the adsorption capacities of contaminants. The as-prepared HPA-GO was characterized by FTIR, TGA, XRD, zeta potential and SEM analyses. To further investigate the interaction mechanism between HPA-GO and contaminants, kinetic, isothermal and thermodynamic studies of Pb(II) and MB adsorption by HPA-GO were carried out. The batch adsorption tests are discussed in detail, and a possible adsorption mechanism has been proposed. In addition, the effect of coexisting ions and the regeneration of HPA-GO have been evaluated for practical applications.

2. Materials and methods

2.1. Chemicals and materials

Poly(ethylene glycol) diglycidyl ether (PEG-DE, Sigma Aldrich, USA) and N-ethylethylene diamine (NEED, Alfa Aesar, London) were used as received. All of the other chemicals, which were obtained from Sinopharm Chemical Reagent Beijing Co., Ltd, China, were of analytical reagent grade. In addition, ultrapure water (EASY-pure LF, Barnstead International, Dubuque, Iowa USA) was used. 0.1 mol L^{-1} HCl and 0.1 mol L^{-1}NaOH were used for pH adjustment. Lead acetate, which was employed as the heavy metal source, and methylene blue (MB), which was employed as the dye source, were dissolved in ultrapure water prior to use.

2.2. Synthesis of hyperbranched polyamine (HPA)

Hyperbranched polyamine (HPA) was synthesized through the nucleophilic ring-opening reaction of PEG diepoxy and amine monomer [29]. The reaction was conducted in a three-neck flask equipped with a nitrogen inlet tube and a reflux condenser. PEG-DE (0.02 mol), NEED (0.02 mol) and ethanol (60 mL) were added to the flask. The mixture was stirred at room temperature for 48 h and then refluxed for an additional 24 h. After most of the ethanol was removed by evaporation, the residue was precipitated in n-hexane to produce a viscous liquid followed by drying in a vacuum oven at 45 °C for 24 h, which resulted in a light yellow liquid with a yield of approximately 92%.

2.3. Synthesis of HPA-modified grapheme oxide (HPA-GO)

Graphene oxide (GO) was prepared from purified natural graphite using the modified Hummers method [30]. HPA-GO was prepared according to the following steps: First, GO (400 mg) was fully dispersed in 150 mL of water under ultrasonication for 6 h at room temperature. Then, HPA (4 g) and KOH (150 mg) were added, and the mixture was vigorously stirred at room temperature for 12 h and 80 °C for an additional 12 h. The color of the solution became darker during the reaction process. Finally, the resulting product was centrifuged (9500 rpm for 20 min) and repeatedly washed with ethanol (two times) and water (two times) to remove the free HPA polymers that were not anchored to the nanosheets. The final product (HPA-GO) was dried in vacuum at 45 °C for 24 h.

2.4. General characterization

The performance of the synthesized product was characterized using several techniques. ^{1}H nuclear magnetic resonance spectroscopy (^{1}H NMR) was performed with a DMX-300 MHz

instrument (Bruker, Germany) using $CDCl_3$ as the solvent to dissolve HPA. The FTIR spectra measurements were mounted by using a Perkin-Elmer Spectrum One FTIR spectrometer (Perkin-Elmer, United States) in KBr pellet at room temperature in a spectral range of 4000–400 cm^{-1}. HPA was coated onto KBr chip for FTIR analysis. While dried GO or HPA-GO powder was grinded with KBr and then pressed into thin slice for FTIR analysis. TGA was performed on a Diamond High Temperature Type TG/DTA thermoanalyzer (Perkin-Elmer, United States) under a N_2 atmosphere from room temperature to 800 °C with heating rate of 10 °C/min. The XRD patterns were acquired on a RigakuD/MAX 2200 X-ray diffractometer (Tokyo, Japan). For zeta potential analysis, 10 mg of HPA-GO powder was dispersed in 50 mL of ultrapure water with various pH values, the obtained solution samples were measured with a JS94H (Shanghai, China). SEM and energy-dispersive X-ray spectroscopy (EDX) were performed using powder samples on a FEI QUANTA FEG250 coupled with INCA Energy X-MAX-50.

2.5. Adsorption experiments

All of the pollutant solutions in the experiment were prepared by dissolving $Pb(CH_3COO)_2$ and MB in ultrapure water. Fresh dilutions were used in each experiment.

To determine the optimum adsorption conditions and study the adsorption mechanism of Pb(II) and MB adsorption, batch adsorption experiments were performed. The prepared adsorbent (HPA-GO) was placed in a beaker containing 50 mL of the Pb(II) or MB aqueous solution and then shaken on a temperature-controlled shaker. The dosage effect was tested in the 2–14 mg range for Pb(II) and 2–16 mg range for MB (contact time was 3 h, temperature was 298 K). The effect of pH was studied in the range of 1–6 for Pb(II) and 1–8 for MB. The effect of the contact time was determined from 20–120 min for Pb(II) and 20–180 min for MB (10 mg dosage was used for both Pb(II) and MB, pH = 6, temperature was 298 K). The adsorption equilibrium isotherms were determined with an initial concentration range of 20–200 mg L^{-1} for both Pb(II) and MB. The adsorption thermodynamics were studied at temperatures ranging from 298 to 318 K with varying initial concentrations.

At the end of the adsorption, the mixed solution was centrifuged, and the supernate was collected to determine the residual concentrations of Pb(II) and MB. The removal efficiency and the amount of Pb(II) and MB adsorbed onto HPA-GO were calculated using the following equations:

$$\text{Removal efficiency } (\%) = 100 \times \frac{C_0 - C_e}{C_0} \quad (1)$$

$$q_t = \frac{(C_0 - C_t)V}{m} \quad (2)$$

where C_0 and C_e (mg L^{-1}) are the initial and equilibrium concentrations of the pollutant, respectively. C_t (mg L^{-1}) is the concentration of adsorbate in the aqueous solution at time t (min). q_t (mg g^{-1}) is the amount of adsorbate adsorbed per unit mass of the adsorbent at time t. V (L) is the volume of the adsorbed solution, and m (g) is the mass of the adsorbent.

2.6. Regeneration of the adsorbent

In the desorption experiments, an HCl solution (50 mL, 0.5 M) and ethanol (50 mL) were used as the desorption agents for Pb(II) and MB, respectively, to regenerate the adsorbents from the HPA-GO loaded with Pb(II) and MB samples, respectively. After shaking for 180 min at 298 K, the samples that were separated from the solution by centrifugation were washed three times with ultrapure water and subjected to the adsorption–desorption process to recycle. The adsorption–desorption cycle was successively conducted 5 times for each test.

2.7. Replication of batch experiment

Each batch adsorption experiment was conducted twice and the data shown are the average values. The individual values were generally within 5%.

3. Results and discussion

3.1. General characterization

The preparation process of HPA-GO and its subsequent adsorption of Pb(II) and MB are shown in Scheme 1. Water-soluble HPA can be obtained through a one-pot reaction of commercial PEG-DE and NEED. The molecular structure was determined based on the ^{1}H NMR spectrum (Fig. 1a). The peaks at 0.8–1.4 ppm corresponded to the signal from the methyl groups. In addition, the characteristic peaks of –CH_2– and –CH– connected to nitrogen and oxygen atoms appeared at 2.03–2.9 ppm and 3.1–4.1 ppm, respectively. The results from the ^{1}H NMR spectrum indicated the successful synthesis of HPA according to the literature [29]. HPA was further used to modify GO through a nucleophilic ring-opening reaction between the amine groups of HPA and the epoxy groups of GO in a KOH solution to introduce hydroxyl and amine groups onto the GO surface to increase the adsorption efficiency of Pb(II) and MB. In addition, due to the good water solubility of HPA grafted

onto the GO surface, it was well dispersed in the aqueous solution, which was helpful for improving the adsorption properties of HPA-GO.

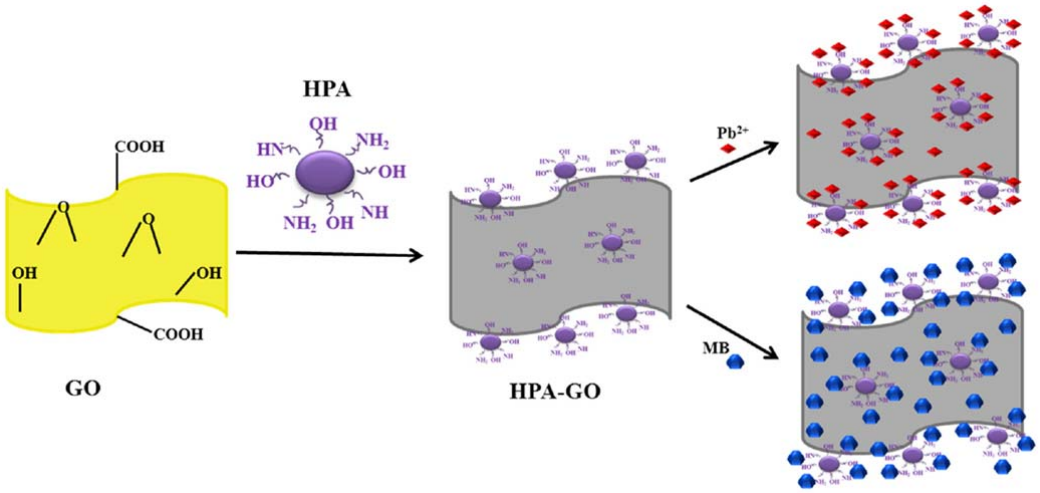

Scheme 1. The process for preparation of HPA-GO and its adsorption of Pb(II) and MB.

The covalent functionalization of graphene oxide with HPA was characterized by FTIR spectroscopy (Fig. 1b). The characteristic peaks in the GO spectrum at 3410, 1739, 1626, 1415 and 1221 cm^{-1} were due to the OH, C═O in –COOH, aromatic C═C, carboxy C–O, and epoxy C–O stretches, respectively [31]. In the HPA spectrum, the broad adsorption band located at 3412 cm^{-1} was due to the stretching vibration of O–H and N–H. Due to the strong absorption of the –OH groups and trace amounts of water, the O–H and N–H groups merged into one broad peak. The two bands located at 2975 cm^{-1} and 2873 cm^{-1} corresponded to the stretching of the $–CH_2–$ groups. The peak at 1656 cm^{-1} corresponded to N–H bending vibration of $–NH_2$[32]. The characteristic peak of the aliphatic C–O ether bond appeared at 1086 cm^{-1}. In the HPA-GO spectrum, the peak located at 1650 cm^{-1} was due to vibration of the aromatic rings and $–NH_2$groups. The peak located at 1221 cm^{-1} that was assigned to epoxy C–O stretches disappeared, suggesting the successful reaction of the epoxy groups on graphene oxide with the amine groups of HPA. In addition, two new bands appeared at 2924 cm^{-1} and 2843 cm^{-1} due to $–CH_2–$ stretching vibrations of HPA, which also indicated the successful grafting of HPA onto the GO surface. It is important to note that the existence of abundant hydroxyl and amine groups as well as ether bonds in HPA have two advantages as follows: first, these functionalities endow HPA with good water solubility, which is beneficial for improving the water dispersity of GO. Second, the abundant hydroxyl and amine groups can interact with heavy metals and dyes [21]. Therefore, grafting of HPA onto GO surface is expected to result in high efficiency removal of heavy metals and dyes.

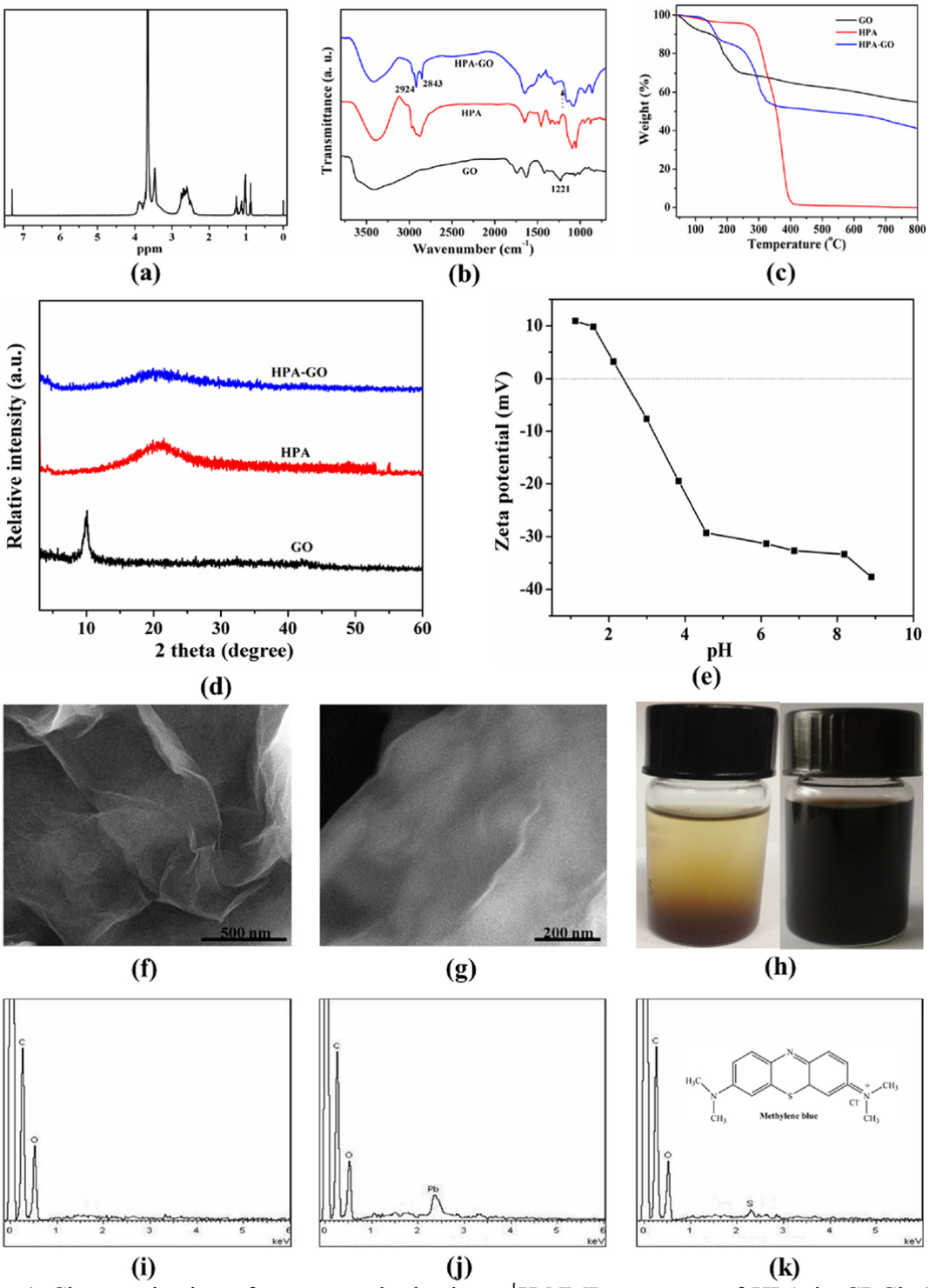

Fig. 1. Characterization of as-prepared adsorbent: ^{1}H NMR spectrum of HPA in $CDCl_3$ (a); FTIR spectra (b), TGA analysis (c), XRD patterns (d) of HPA, GO, HPA-GO; Zeta potential of HPA-GO (e); SEM images of GO (f), HPA-GO (g), photographs for the dispersion status of GO (left) and HPA-GO (right) in water settled for 2 h and 2 months, respectively (h); EDX analysis of HPA-GO before (i) and after loading with Pb(II) (HPA-GO-Pb(II), j) and MB (HPA-GO-MB, k).

The weight loss curves for GO, HPA and HPA-GO obtained from TGA are shown inFig. 1c. The weight loss of GO started below 100 °C due to the volatilization of adsorbed water. A relatively large weight loss was observed at approximately 195 °C, which was attributed to the decomposition of oxygen-containing functional groups. In contrast, HPA exhibited a weight loss stage from 260 °C to 450 °C, which appear to be effective in enhancing the thermal stability of the GO sheets. For HPA-GO, the maximum weight loss temperature (300 °C) and the residue at 800 °C (41.3%) is located between those of neat GO (195 °C, 55.1%) and HPA (360 °C, 0.2%), indicating that HPA has been successfully grafted onto the GO surfaces. Therefore, the nanocomposite adsorbent exhibited good thermal stability, which is beneficial for the application of the adsorbent.

The wide-angle XRD patterns of GO and HPA-GO are shown in Fig. 1d. In comparison to the pure GO diffraction signals, no diffraction signals corresponding to GO in the HPA-GO composites were observed at 10°. This results may be due to the grafting of a number of HPA polymers onto the GO surfaces, which extends the layer distance of GO and reduces the orderly aggregation of the GO sheets resulting in more fewer-layered GOs and weaker peaks from carbon. In addition, a broad diffraction peak corresponding to amorphous HPA appeared in the pattern of HPA-GO. The results from the XRD analysis also indicated that HPA was anchored onto the GO nanosheets.

Zeta potentials are widely used to analyze the electronic charges on the surface of adsorbents in aqueous solutions. The point of zero charge (pHzpc) of HPA-GO was determined by measuring the zeta potential of the nanocomposite as a function of pH[33]. As shown in Fig. 1e, the pHzpc of HPA-GO was 2.4, and the surface of HPA-GO was negatively charged due to the deprotonation of the hydroxyl groups when the pH was higher than 2.4. The pH of intrinsic water typically ranges from 7 to 9 [34]. Therefore, the as-prepared HPA-GO will be negatively charged in most natural water environments. Because the adsorption process of cation pollutants, such as heavy metal ions and cation dyes, is typically dominated by electrostatic interactions, HPA-GO is expected to exhibit improved adsorption capacities, and the performance of the adsorbents will increase in more alkaline conditions.

The SEM images showed the microstructure of GO (Fig. 1f) and HPA-GO (Fig. 1g). GO possessed a paper-like folded structure with thin layers. After the introduction of HPA, the surface of layered HPA-GO was smoother and thicker compared to that of GO.

Due to the introduction of water-soluble HPA, HPA-GO was easily dissolved in water using ultrasonication. Fig. 1h shows the dispersion state of GO and HPA-GO in water (2 mg mL^{-1}) at room temperature after settling for different periods of time. HPA-GO can be uniformly dispersed in water to form homogenous and stable solutions, and then, the dispersions were allowed to settle for at least two months without obvious precipitants (Fig. 1h right). However, GO cannot be well dispersed in water, and precipitates formed in 2 h after ultrasonication (Fig. 1h left). Therefore, the improved solubility of HPA-GO further supports the successful functionalization of GO sheets.

EDX analysis was used to analyze the elemental composition of the sorbent before and after adsorption. Based on the results shown in Fig. 1i, C and O existed in the spectrum of HPA-GO prior to adsorption. After adsorption of Pb(II) and MB onto HPA-GO, new peaks corresponding to Pb and S appeared in the spectrum of HPA-GO-Pb(II) (Fig. 1j) and HPA-GO-MB (Fig. 1k), respectively. These results qualitatively indicate that Pb(II) and MB were successfully adsorbed onto HPA-GO.

3.2. Factors affecting adsorption

3.2.1. Effect of dosage on the removal efficiency

The effect of the adsorbent dosage on the removal efficiency was investigated by adding various amounts of the HPA-GO nanocomposite to 50 mL of Pb(II) and MB solutions (60 mg L^{-1}) followed by shaking for 3 h at room temperature (Fig. 2a). The removal efficiency of Pb(II) and MB increased as the adsorbent dosage increased, which was due to more adsorption sites being available at higher adsorbent dosages. However, when the adsorption process reach a saturated state, no more Pb(II) and MB can be adsorbed onto the adsorbent even if the dosage of the adsorbent is increased. As indicated by the results, the removal efficiency reached an equilibrium at 98.4% and 97.6% for Pb(II) and MB, respectively, corresponding to 0.01 g HPA-GO dosage. Considering the removal efficiency and practicality, the optimal adsorbent dosage was maintained at 0.01 g for Pb(II) and MB in all subsequent experiments.

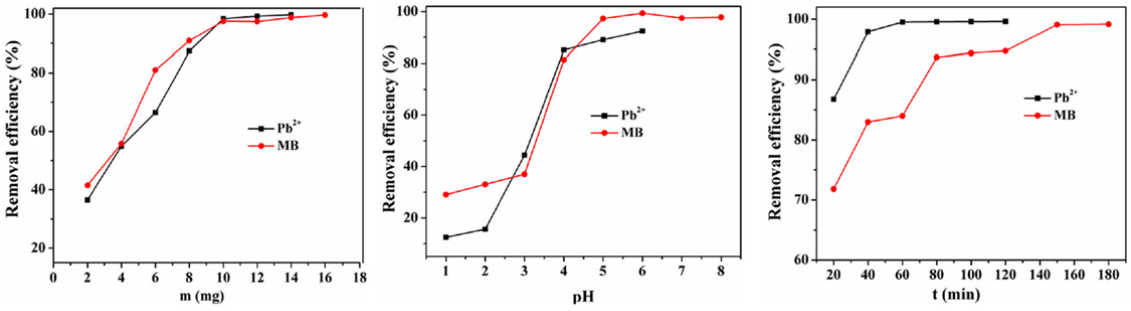

Fig. 2. Effect of dosage (a), pH (b) and contact time (c) on adsorption behavior of Pb(II) (C_0 = 60 mg L^{-1},V = 50 mL, temperature at 298 K) and MB (C_0 = 60 mg L^{-1}, V = 50 mL, temperature at 298 K).

3.2.2. Effect of pH on the removal efficiency

Because pH has been reported as a key condition that affects the adsorption performance of heavy metal ions and dyes from aqueous solution [35], a series of batch equilibrium tests were carried out to confirm the effect of pH on Pb(II) and MB adsorption by HPA-GO in a wide range of pH values. Fig. 2b shows the uptake of Pb(II) and MB onto HPA-GO as a function of the corresponding solution pH. When the pH values of the solutions were less than 2.0, the surface functional groups on HPA-GO were protonated resulting in a positively charged surface [36], which was consistent with the zeta potential obtained from in Fig. 1e. The adsorption capacities of Pb(II) and MB were low due to electrostatic repulsion [37]. As the pH values increased, the surface charge of HPA-GO became more negative, and the adsorption capacities of Pb(II) and MB substantially increased due to electrostatic attractions between the oppositely charged ions. However, when the pH values were higher than 6.1, hydrolysis of Pb(II) occurs, resulting in the formation of $Pb(OH)_2$[38]. Under these condition, the removal mechanism of Pb(II) would become more complicated, and it would be difficult to distinguish between the adsorption and precipitation of Pb(II) removed from solutions. Therefore, a pH of 6.1 was chosen for subsequent adsorption experiments for Pb(II) to avoid precipitation of $Pb(OH)_2$. In addition, as shown in Fig. 2b, the maximum removal efficiency (99%) was achieved at a solution pH of 5.9 for MB. Therefore, the high surface charge density that was generated on HPA-GO under high pH conditions, which was translated into a low zeta potential, resulted in an increase in the adsorption capacity for MB^+[39]. In addition, the pH value of the original MB solution was measured to be approximately 6.0. Based on the removal efficiency and simple operation, subsequent experiments were carried out with the original MB solution.

3.2.3. Effect of contact time on the removal efficiency

The contact time between the adsorbent and adsorbate is an important parameter for evaluating the adsorption performance of adsorbents. Fig. 2c shows the influence of the contact time on the removal efficiency of Pb(II) and MB. In general, a longer contact time was advantageous for achieving higher removal efficiencies of Pb(II) and MB. Absorption is a time-consuming process, and an increase in the contact time is beneficial for sufficient interactions between Pb(II)/MB and the adsorption sites of HPA-GO. For Pb(II) adsorption, the removal efficiency increased sharply within 40 min and reached equilibrium in 60 min. For MB adsorption, the removal efficiency increased sharply within 80 min and reached equilibrium in 150 min. In the initial stage of the adsorption reaction, the adsorption sites on HPA-GO for Pb(II)/MB were sufficient. As time progressed, more and more adsorption sites were occupied, and the adsorption capacity was eventually saturated. Therefore, 60 min and 150 min were selected as the optimum contact time for Pb(II) and MB, respectively.

3.3. Adsorption kinetics

The pseudo-first order, pseudo-second order, intraparticle diffusion and Bangham equations were applied to describe the kinetics of the contaminant adsorbing onto HPA-GO [40], [41], [42] and [43]. Each model is expressed as follows:

Pseudo-first order model:

$$\ln(q_e - q_t) = \ln\ q_e - k_1 t \tag{3}$$

Pseudo-second order model:

$$\frac{t}{q_t} = \frac{1}{k_2 q_e^2} + \frac{t}{q_e} \tag{4}$$

Intraparticle diffusion model:

$$q_t = k_{dif} t^{1/2} + C \tag{5}$$

Bangham model:

$$\ln q_t = \ln\ k_b + \left(\frac{1}{m}\right) \ln\ t \tag{6}$$

where q_e and q_t (mg g^{-1}) are the amounts of pollutants adsorbed onto the adsorbent at equilibrium and at time t (min), respectively. k_1 and k_2 (mg min g^{-1}) are the pseudo-first order and pseudo-second order rate constant, respectively. k_{dif} (mg g^{-1} $min^{-1/2}$) is the intraparticle diffusion rate constant. m and k_b are the related constants of the Bangham model.

The linear fitting results of the kinetic data are shown Fig. 3, and the relevant calculated results are listed in Table 1. The pseudo-second order kinetic model fitted well with all of the experimental data compared to the three other models (Pb(II): $R^2 = 0.9995$, MB:$R^2 = 0.9984$), which indicated that the adsorption rate was primarily determined by a chemical adsorption process. This result implied that electron transfer, exchange or sharing was generated and a chemical bond was formed in the adsorption process [44]. In addition, the calculated q_e from the pseudo-second order kinetic model was 301.8 mg g^{-1} for Pb(II) and 299.5 mg g^{-1} for MB, which are consistent with the experimental data (298.9 mg g^{-1} for Pb(II) and 297.5 mg g^{-1} for MB).

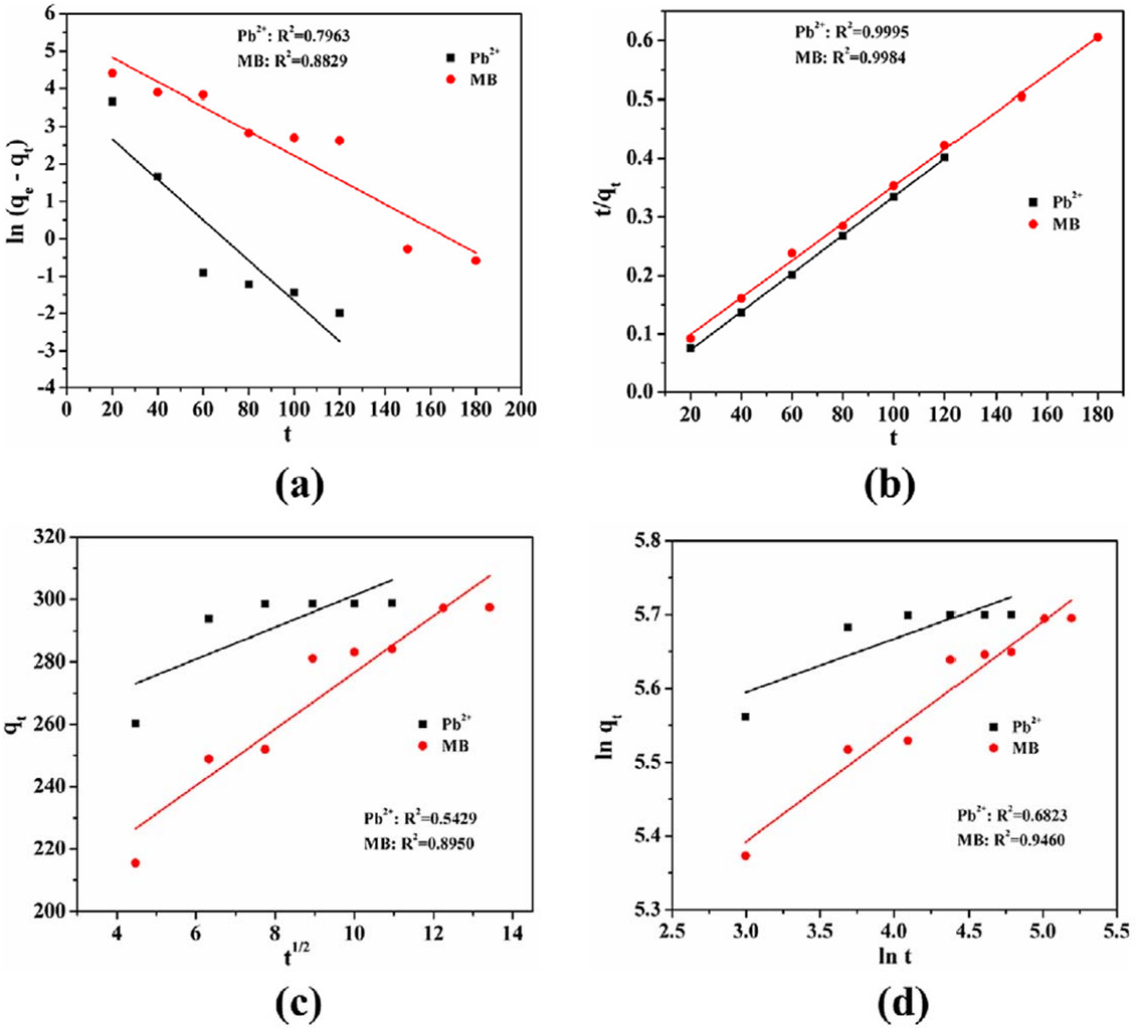

Fig. 3. Pseudo-first-order kinetics (a), pseudo-second-order kinetics (b), Intraparticle diffusion kinetics (c) and Bangham kinetics (d) for adsorption of Pb(II) (m = 10 mg, C_0 = 60 mg L^{-1}, V = 50 mL, pH at 6.1, temperature at 298 K) and MB (m = 10 mg, C_0 = 60 mg L^{-1}, V = 50 mL, pH at 5.9, temperature at 298 K).

Table 1. Constants and correlation coefficients for the kinetic models of Pb(II) and MB onto HPA-GO.

Kinetic model	Parameter	Pb(II)	R^2	MB	R^2
Pseudo-first-order	k_1 (mg min g^{-1})	0.0541	0.7963	0.0229	0.8829
	q_e (mg g^{-1})	42.28		171.01	
Pseudo-second-order	k_2 (mg min g^{-1})	0.0014	0.9995	0.0003	0.9984
	q_e (mg g^{-1})	305.81		299.53	
Intraparticle diffusion	k_{dif} (mg g^{-1} $min^{-1/2}$)	5.1043	0.5429	5.5445	0.8950
Bangham	m	13.8889	0.6823	6.7083	0.9460
	k_b (mg g^{-1})	216.8379		140.5102	

3.4. Adsorption isotherms

The adsorption isotherms were investigated to provide insight into how an adsorption system reaches dynamic equilibrium and how the adsorbate interacts with adsorbent surface [45]. Four isotherm equations were selected to model the adsorption isotherm data including the Henry [46], Langmuir [47], Freundlich [48] and Temkin [49] equations, which can be expressed as follows:

Henry equation:

$$q_e = K_H C_e \quad (7)$$

Langmuir equation:

$$\frac{C_e}{q_e} = \frac{1}{bq_m} + \frac{C_e}{q_m} \quad (8)$$

Freundlich equation:

$$\ln q_e = \ln K_F + \frac{1}{n} \ln C_e \quad (9)$$

Temkin equation:

$$q_e = \frac{RT}{b_T} \ln C_e + \frac{RT}{b_T} \ln A_T \quad (10)$$

where q_m (mg g^{-1}) is the maximum adsorption capacity. K_H and K_F are the constants related to the adsorption capacity and intensity, respectively. b (L mg^{-1}) is the Langmuir constant related to the affinity of the binding site. A smaller $1/n$ value indicates a more heterogeneous surface. However, a value closer to or equal to one indicates the adsorbent has relatively more homogeneous binding sites. $\frac{RT}{b_T}$ is related to the adsorption heat. A_T is the equilibrium constant corresponding to the maximum binding energy.

The fitting results obtained from these four common adsorption models are shown in Fig. 4, and the calculated isotherm constants are listed in Table 2. According to the correlation coefficients (R^2), the Langmuir model is more suitable than the three other models for describing the adsorption of both Pb(II) ($R^2 = 0.9994$, $R^2 = 0.9949$,$R^2 = 0.9982$) and MB ($R^2 = 0.9962$, $R^2 = 0.9971$, $R^2 = 0.9933$) at 298 K, 308 K and 318 K, respectively.

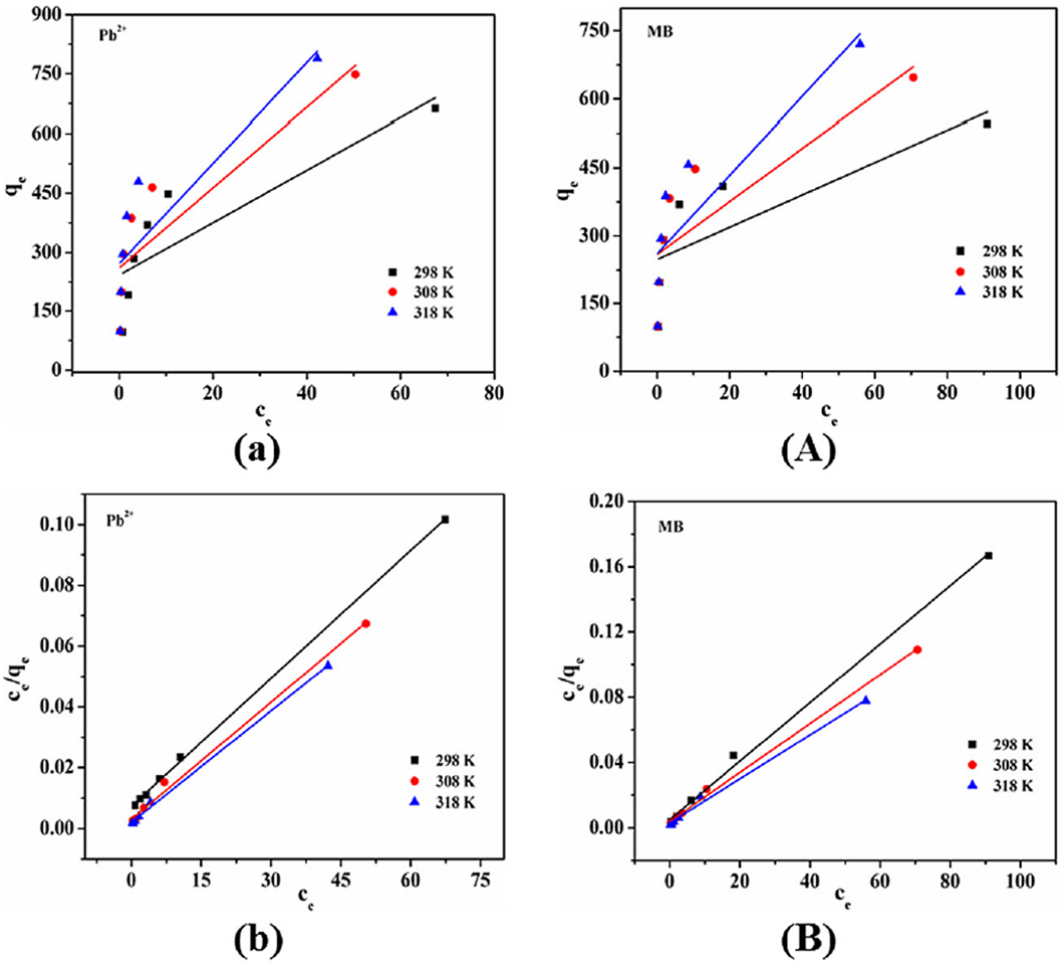

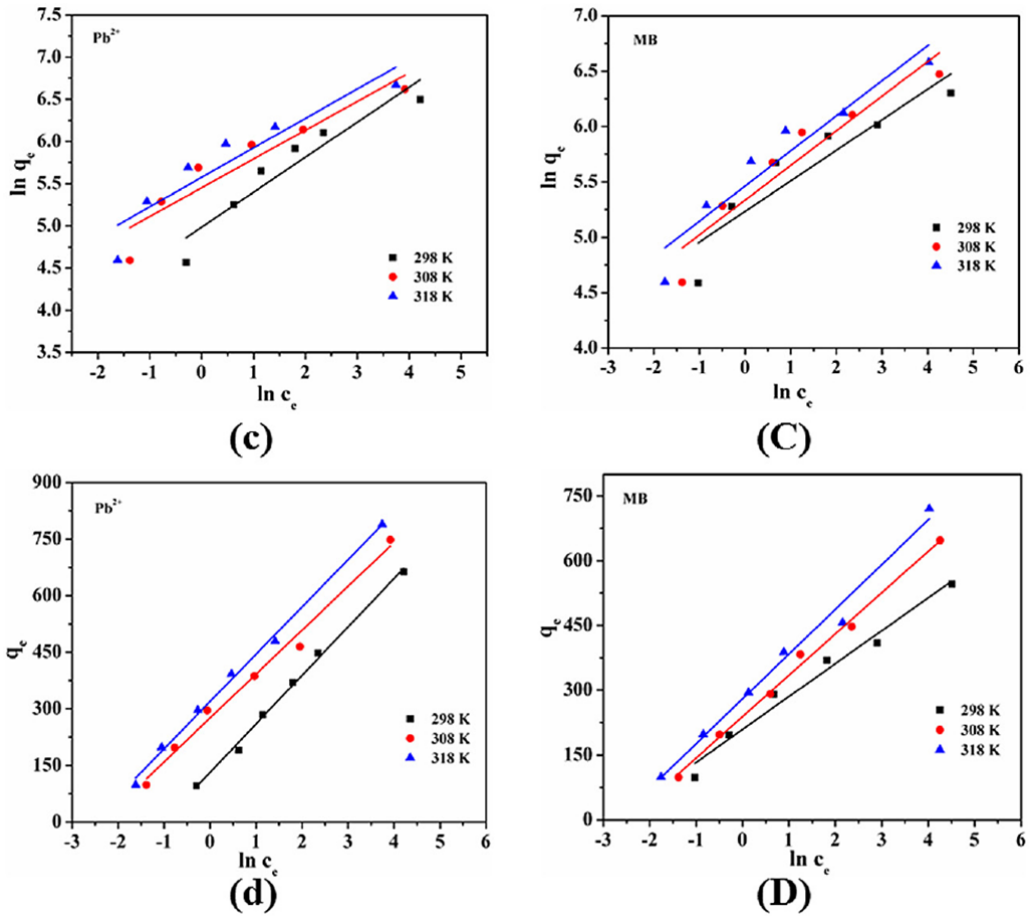

Fig. 4. Henry (a), Langmuir (b), Freundlich (c) and Temkin (d) adsorption isotherm fit of Pb(II) (m = 10 mg, C_0 = 20–200 mg L^{-1}, V = 50 mL, pH at 6.1, contact time for 60 min, temperature at 298 K, 308 K and 318 K, respectively) and Henry (A), Langmuir (B), Freundlich (C) and Temkin (D) adsorption isotherm fit of MB (m = 10 mg, C_0 = 20–200 mg L^{-1}, V = 50 mL, pH at 5.9, contact time for 150 min, temperature at 298 K, 308 K and 318 K, respectively).

These results indicated that the surface of HPA-GO has a monolayer coverage of Pb(II) or MB, and the reaction interface between Pb(II)/MB and HPA-GO was nonhomogeneous [50]. The maximum adsorption amount calculated from the Langmuir model was 819.7 mg g^{-1} for Pb(II) and 740.7 mg g^{-1} for MB at 318 K. A smaller 1/n value (<0.5) indicated that Pb(II) or MB was easily adsorbed onto the heterogeneous surface of the HPA-GO composite. In addition, for Pb(II) and MB adsorption onto HPA-GO, the correlation coefficients for the Temkin isotherm model were all higher than 0.97, which indicated that the adsorption was based on heat [51]. The adsorption capacity listed inTable 2 increased as the temperature increased, which was due to an increase in the diffusion rate of the adsorbate across the external boundary layer caused by the temperature increasing [52].

Table 2. Adsorption isotherm parameters for Pb(II) and MB adsorption onto HPA-GO at 298 K, 308 K, 318 K.

Temperature	Adsorption isotherm	Parameter	Pb(II)	R^2	MB	R^2
298 K	Henry	K_H	6.619	0.6640	3.555	0.5365
	Langmuir	b (L mg^{-1})	0.1902	0.9994	0.3616	0.9962
		q_m (mg g^{-1})	714.29		558.66	
	Freundlich	K_F	146.03	0.8550	187.59	0.8194
		$1/n$	0.4154		0.2752	
	Temkin	b_T	19.30	0.9950	32.56	0.9705
		A_T	2.793		15.680	
308 K	Henry	K_H	10.118	0.7114	5.827	0.6141
	Langmuir	b (L mg^{-1})	0.4286	0.9949	0.3856	0.9971
		q_m (mg g^{-1})	775.19		666.67	
	Freundlich	K_F	233.25	0.8565	207.65	0.8775
		$1/n$	0.3405		0.3123	
	Temkin	b_T	22.02	0.9863	26.78	0.9933
		A_T	10.71		12.176	
318 K	Henry	K_H	12.673	0.6971	8.635	0.6959
	Langmuir	b (L mg^{-1})	0.5922	0.9982	0.4470	0.9933
		q_m (mg g^{-1})	819.67		740.74	
	Freundlich	K_F	263.87	0.8413	235.83	0.8914
		$1/n$	0.3488		0.3166	
	Temkin	b_T	21.11	0.9956	25.52	0.9841
		A_T	12.82		14.926	

3.5. Thermodynamic parameters

To further investigate the effect of the temperature on the adsorption and explore the mechanism involved in the adsorption process, the thermodynamic behavior was evaluated using the following equations:

$$\Delta G = -RT \ln K_d \quad (11)$$

$$\ln K_d = \frac{\Delta S}{R} - \frac{\Delta H}{RT} \quad (12)$$

where R (8.314 J mol^{-1} K^{-1}) is the gas constant, T (K) is the absolute temperature and K_d is the thermodynamic equilibrium constant. ΔS is the entropy change, ΔH is the enthalpy change, and ΔG is the Gibbs free energy change in a given process (kJ mol^{-1}). The ΔS, ΔH and ΔG results are shown in Table 3. The negative values of ΔG at the three temperatures indicated that the adsorptive forces were sufficiently strong to overcome the potential barrier. The adsorption process was spontaneous, and improved adsorption performance can be achieved at a higher temperature. The positive values of ΔH suggested that the adsorption process was endothermic in nature. In addition, the adsorption capacity of Pb(II) and MB

would increase as the temperature increased. The positive values of ΔS implied increased randomness at the solid-solution interface and good affinity of Pb(II) and MB with HPA-GO.

Table 3. Thermodynamic parameters for Pb(II) and MB adsorption onto HPA-GO.

Pollutants	**Temperature**	**lnK_d**	**ΔG (kJ mol^{-1})**	**ΔH (kJ mol^{-1})**	**ΔS (J mol^{-1} K^{-1})**
Pb(II)	298 K	1.717643	−4.256	10.261	48.960
	308 K	1.942880	−4.975		
	318 K	1.976137	−5.225		
MB	298 K	1.964634	−4.868	1.482	21.273
	308 K	1.970714	−4.965		
	318 K	2.002559	−5.128		

3.6. Adsorption mechanism

The FTIR spectra of HPA-GO before and after loading Pb(II) and MB (referred to as HPA-GO-Pb and HPA-GO-MB, respectively) were recorded to gain insight into the adsorption mechanism (Fig. 5). A possible mechanism has been proposed in Scheme 2. For Pb(II) removal, based on the zeta potential results, the protonation of the amino groups led to a positively charged HPA-GO surface when the solution pH value was less than 2.4. Therefore, the adsorption interaction may involve chelation of the amino and hydroxyl groups of HPA-GO and lead [21] and [53]. By increasing the solution pH, deprotonation begins, and a new electrostatic attraction may form among the negatively charged surface HPA-GO and the lead ions. This interaction can also be confirmed by the FTIR spectra shown in Fig. 5. The peaks at 3420 cm^{-1} and 1650 cm^{-1}, which are due to the stretching vibration of the O–H (or N–H) groups and the bending vibration of the –NH_2groups (before adsorption-spectrum HPA-GO), shifted to 3408 cm^{-1} and 1600 cm^{-1}(after adsorption-spectrum HPA-GO-Pb), respectively, indicating that all of these groups may interact with Pb(II) [54] and [55].

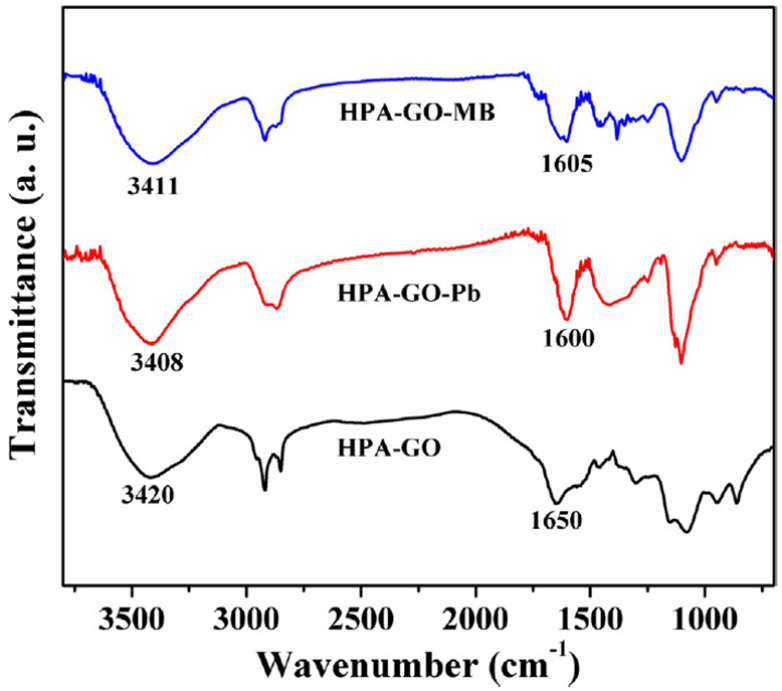

Fig. 5. FTIR spectra of HPA-GO before and after loading Pb(II) (HPA-GO-Pb) and MB (HPA-GO-MB).

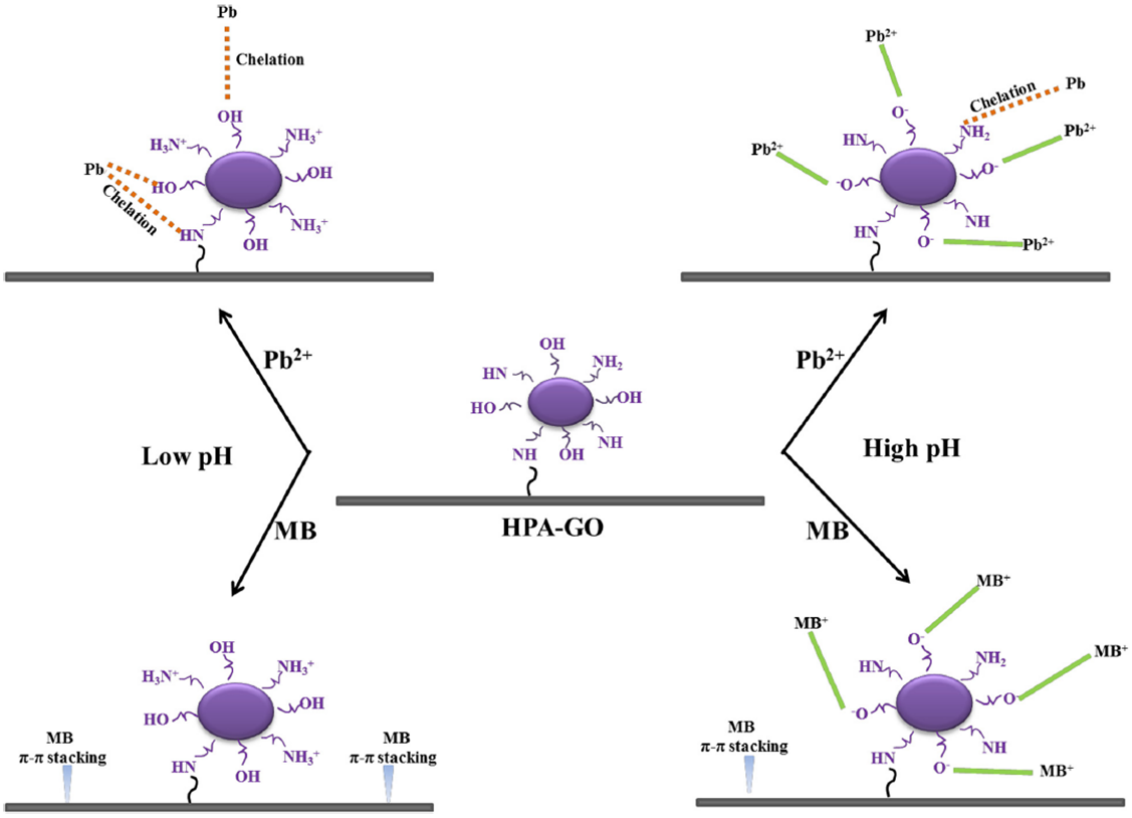

Scheme 2. Proposed adsorption mechanism of Pb(II) and MB adsorption onto HPA-GO.

The removal of MB improved as the solution pH increased. In very acidic media (pH $\leqslant$ 2.4), the electrostatic repulsion between the positively charged HPA-GO and the MB^+ molecules weakened the adsorption strength [56] and [57]. However, the removal efficiency still reached 33% when the solution pH was 2. This result may be due to both MB and HPA-GO possessing abundant aromatic rings, and π–π stacking interactions may occur between MB molecules and HPA-GO, resulting in effective removal of MB[58] and [59]. This interaction can be verified by the FTIR spectra shown in Fig. 5. The adsorption peak corresponding to the aromatic rings in HPA-GO shifted from 1650 cm^{-1}(before adsorption-spectrum HPA-GO) to 1605 cm^{-1} (after adsorption-spectrum HPA-GO-MB) due to π–π stacking interactions [60]. When the solution pH increased further, electrostatic attractions between the negatively charged HPA-GO and cationic MB dyes formed, which increased the adsorption capacity of MB [61]. The peak corresponding to the –OH groups at 3421 cm^{-1} shifted to 3411 cm^{-1} and may explain the interaction between the dissociated hydroxyls groups and MB^+ [55].

3.7. Performance evaluation

In addition, a comparison of the maximum adsorption capacities (q_{max}) of HPA-GO with other reported adsorbents for Pb(II) and MB was performed to illustrate the excellent adsorption performance of HPA-GO (Table 4). The maximum adsorption capacities of HPA-GO for Pb(II) and MB were higher than those of other adsorbents. First, GO nanosheets have a high specific surface area and large number of functional groups that provide reaction sites for grafting of HPA molecules. Therefore, the existence of GO in HPA-GO increases the contact area between the adsorbent and adsorbate. Second, grafting of water-soluble HPA endowed HPA-GO with good water dispersity and abundant hydroxyl and amine groups, which can strengthen the interaction between the adsorbent and the adsorbate. Therefore, HPA-GO can effectively improve the adsorption capacity of Pb(II) and MB. Based on the convenient synthetic process and good adsorption performance, HPA-GO is a good absorbent for treating polluted water.

Basic cations, such as K^+, Na^+, Ca^{2+} and Mg^{2+}, are common metal ions in both natural water resources and heavy metal wastewater from industrial sources. Their presence may compete with Pb(II) for binding at the adsorption sites on the surface of HPA-GO. The effect of these cations on Pb(II) adsorption was investigated using KNO_3, $NaNO_3$, $Ca(NO_3)_2$ and $Mg(NO_3)_2$ as the ionic medium. Based on the results shown in Fig. 6, the concentration of

coexisting ions increased, the removal efficiency of Pb(II) decreased slightly, which indicated that the high-concentration coexisting ions had weak interferences to the Pb(II) adsorption.

Table 4. Asorption capacities of various adsorbents for Pb(II) and MB.

Material	Target element	Isotherm	q_m (mg g^{-1})	Refs.
HPA-GO	Pb(II)	Langmuir	819.7	This paper
	MB		740.7	
LS-GO-PANI	Pb(II)	Langmuir	216.4	[21]
PDA-GO	Pb(II)	Langmuir	53.6	[24]
GO-ethylenediamine triacetic acid	Pb(II)	Langmuir	454.6	[62]
EDTA-mGO	Pb(II)	Langmuir	508.4	[63]
Chitosan/magnetite composite beads	Pb(II)	Langmuir	63.3	[64]
Chitosan functionalized with xanthate	Pb(II)	Langmuir	322.6	[65]
β-CD/PAA/GO	MB	Langmuir	248	[23]
SBA/HPG-COOH	MB	Langmuir	159.9	[26]
PANF-g-HPEI	MB	Langmuir	161	[27]
GO	MB	Langmuir	351	[59]
MCGO	MB	Langmuir	95.1	[66]
GO sponge	MB	Langmuir	389.8	[67]
Graphene	MB	Langmuir	153.9	[68]

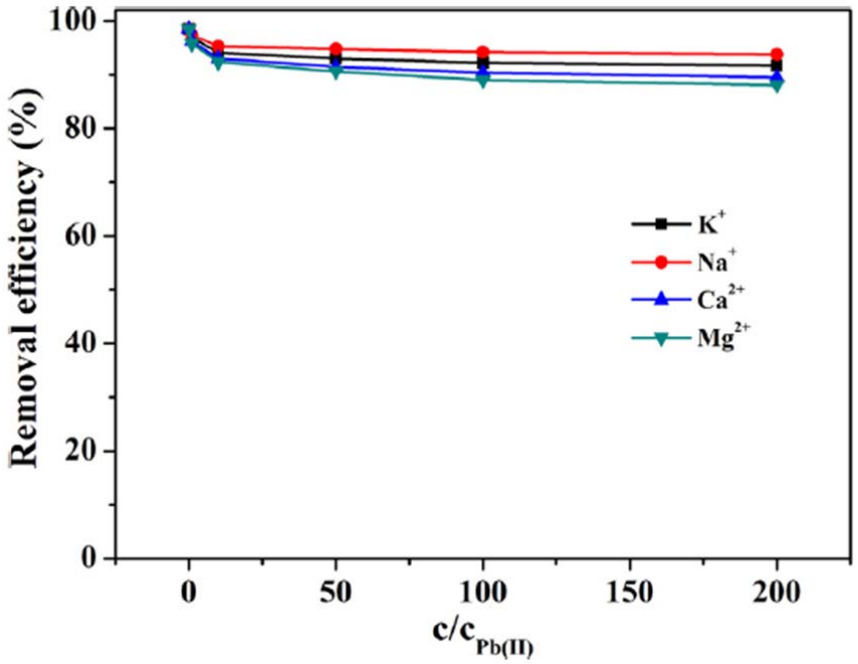

Fig. 6. Effect of coexisting ions on adsorption of Pb(II) (the initial concentration of Pb(II) ($c_{Pb(II)}$) was 60 mg L^{-1}. The concentration ratio of coexisting ions (K^+, Na^+, Ca^{2+} or Mg^{2+}) to Pb(II) ($c/c_{Pb(II)}$) was 0, 1, 10, 50, 100 and 200, respectively. V = 50 mL, pH = 6, temperature at 298 K).

From a practical point of view, regeneration or desorption of pollutants from the sorbent results in a more economical sorption process. The regeneration and reuse of adsorbents is an important factor for evaluating their performance for practical applications. Inexpensive reagents (i.e., HCl solutions (0.5 M) and ethanol) can be used as desorption agents to recover Pb(II) and MB, respectively, from the HPA-GO adsorbent. As shown in Fig. 7, the regenerated HPA-GO exhibited an acceptable removal efficiency for these two pollutants with low decline after 5 adsorption–desorption recycling experiments. Therefore, HPA-GO exhibited the potential for easy recycling and reuse for wastewater treatment.

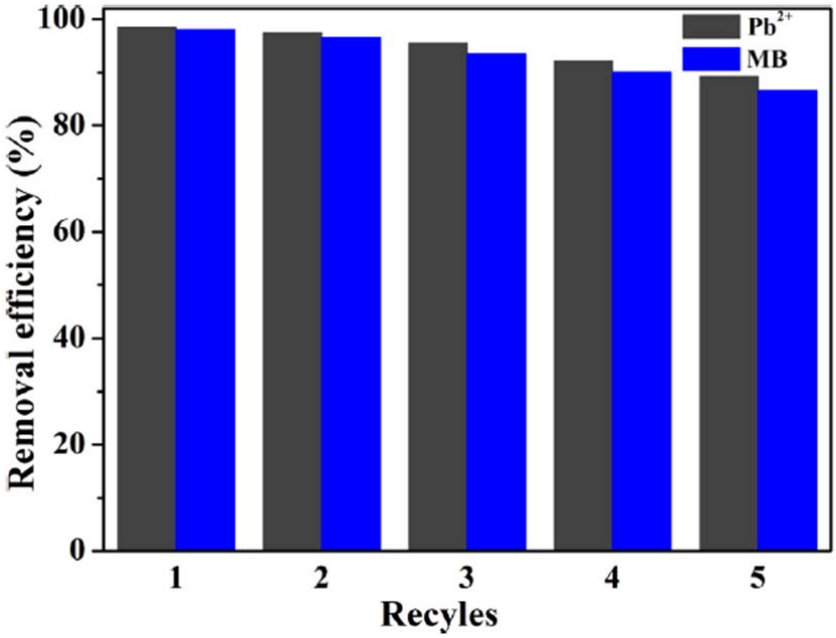

Fig. 7. Adsorption–desorption recycles (m = 10 mg, V = 50 mL, pH = 6, temperature at 298 K, the initial concentration of Pb(II) and MB were 60 mg L^{-1}, respectively).

4. Conclusions

In this study, a simple and effective approach based on surface modification of grapheme oxide with a multifunctional hyperbranched polyamine was developed to obtain a HPA-GO adsorbent. HPA-GO performed well for the adsorption of Pb(II) and MB from aqueous solutions. The equilibrium adsorption capacity of HPA-GO was 819.7 mg g^{-1} for Pb(II) and 740.7 mg g^{-1} for MB at 318 K. The results form the adsorption kinetics and isotherm studies indicated that the adsorption processes of these two types of pollutants fitted well with the pseudo-second order equation and Langmuir model, respectively. In addition, the thermodynamic studies indicated that the adsorption process was endothermic and spontaneous in nature. Importantly, HPA-GO can be easily regenerated by inexpensive

reagents and exhibited considerable adsorption capacity after multiple adsorption–desorption cycles. Based on the high efficiency and feasibility, HPA-GO is a promising absorbent for water purification.

Acknowledgments

This study was supported by the Natural Science Foundation of Shandong Province (No.ZR2013EMQ001), the National Natural Science Foundation of China (Nos. 21175057, 21375047 and 21377046), the Science and Technology Plan Project of Jinan (No.201307010), the Science and Technology Development Plan of Shandong Province (No.2014GSF120004), and QW thanks the Special Foundation for Taishan Scholar Professorship of Shandong Province and UJN (No. ts20130937).

References

[1] K. Miksch, G. Cema, P.F.-X. Corvini, E. Felis, A. Sochacki, J. Surmacz-Gorska, J. Wiszniowski, S. Zabczynski, R&D priorities in the field of sustainable remediation and purification of agro-industrial and municipal wastewater, New Biotechnol. 32 (2015) 128–132.

[2] L. Järup, Hazards of heavy metal contamination, Brit. Med. Bull. 68 (2003) 167– 182.

[3] H. Zollinger, Color chemistry: synthesis, properties and applications of organic dyes and pigments, (1987).

[4] F. Fu, Q. Wang, Removal of heavy metal ions from wastewaters: a review, J. Environ. Manage. 92 (2011) 407–418.

[5] E. Forgacs, T. Cserhati, G. Oros, Removal of synthetic dyes from wastewaters: a review, Environ. Int. 30 (2004) 953–971.

[6] K.K. Christian, H. Seema, M. Saleh, N. Le, K. Mahesh, V. Chandra, K. Kim, Environmental applications using grapheme composites: water remediation and gas adsorption, Nanoscale 5 (2013) 3149–3171.

[7] V.K. Gupta, P.J.M. Carrott, M.M.L. Ribeiro Carrott, R.C. Suhas, Low-cost adsorbents: growing approach to wastewater treatment-a review, Environ. Sci. Technol. 39 (2009) 783–842.

[8] A. Chojnacki, K. Chojnacka, J. Hoffmann, H. Gorecki, The application of natural zeolites for mercury removal: from laboratory tests to industrial scale, Miner. Eng. 17 (2004) 933–937.

[9] W.U. Senevirathna, H. Zhang, B. Gu, Effect of carboxylic and thiol ligands (oxalate, cysteine) on the kinetics of desorption of Hg(II) from kaolinite, Water Air Soil Pollut. 215 (2011) 573–584.

[10] Y. Zhang, Y.F. Li, L.Q. Yang, X.J. Ma, L.Y. Wang, Z.F. Ye, Characterization and adsorption mechanism of Zn2+ removal by PVA/EDTA resin in polluted water, J. Hazard. Mater. 178 (2010) 1046–1054.

[11] S. Wang, H. Sun, H.M. Ang, M.O. Tadé, Adsorptive remediation of environmental pollutants using novel grapheme-based nanomaterials, Chem. Eng. J. 226 (2013) 336–347.

[12] J. Xu, L. Wang, Y. Zhu, Decontamination of bisphenol A from aqueous solution by graphene adsorption, Langmuir 28 (2012) 8418–8425.

[13] M.S. Mauter, M. Elimelech, Environmental applications of carbon-based nanomaterials, Environ. Sci. Technol. 42 (2008) 5843–5859.

[14] Y. Xu, H. Bai, G. Lu, C. Li, G. Shi, Flexible graphene films via the filtration of water-soluble noncovalent functionalized grapheme sheets, J. Am. Chem. Soc. 130 (2008) 5856–5857.

[15] X. Yang, Y. Tu, L. Li, S. Shang, X. Tao, Well-dispersed chitosan/graphene oxide nanocomposites, ACS Appl. Mater. Interfaces 2 (2010) 1707–1713.

[16] M. Bhaumik, A. Maity, V.V. Srinivasu, M.S. Onyango, Removal of hexavalent chromium from aqueous solution using polypyrrole-polyaniline nanofibers, Chem. Eng. J. 181–182 (2012) 323–333.

[17] S. Kagaya, H. Miyazaki, M. Ito, K. Tohda, T. Kanbara, Selective removal of mercury(II) from wastewater using polythioamides, J. Hazard. Mater. 175 (2010) 1113–1115.

[18] K.D. Demadis, A. Stathoulopoulou, Solubility enhancement of silicate with polyamine/polyammonium cationic macromolecules: relevance to silica-laden process waters, Ind. Eng. Chem. Res. 45 (2006) 4436–4440.

[19] F. Ge, M.M. Li, H. Ye, B.X. Zhao, Effective removal of heavy metal ions Cd^{2+}, Zn^{2+}, Pb^{2+}, Cu^{2+} from aqueous solution by polymer-modified magnetic nanoparticles, J. Hazard. Mater. 211–212 (2012) 366–372.

[20] R.S. Vieira, M.M. Beppu, Dynamic and static adsorption and desorption of Hg (II) ions on chitosan membranes and spheres, Water Res. 40 (2006) 1726–1734.

[21] J. Yang, J.X. Wu, Q.F. Lü, T.T. Lin, Facile preparation of lignosulfonate–graphene oxide–polyaniline ternary nanocomposite as an effective adsorbent for Pb(II) ions, ACS Sustainable Chem. Eng. 2 (2014) 1203–1211.

[22] S.W. Zhang, M.Y. Zeng, W.Q. Xu, J.X. Li, J. Li, J.Z. Xu, X.K. Wang, Polyaniline nanorods dotted on graphene oxide nanosheets as a novel super adsorbent for Cr(VI), Dalton Trans. 42 (2013) 7854–7858.

[23] J.S. Liu, G.N. Liu, W.X. Liu, Preparation of water-soluble b-cyclodextrin/poly (acrylic acid)/grapheme oxide nanocomposites as new adsorbents to remove cationic dyes from aqueous solutions, Chem. Eng. J. 257 (2014) 299–308.

[24] Z.H. Dong, D. Wang, X. Liu, X.F. Pei, L.W. Chen, J. Jin, Bio-inspired surface functionalization of grapheme oxide for the adsorption of organic dyes and heavy metal ions with a superhigh capacity, J. Mater. Chem. A 2 (2014) 5034–5040.

[25] C. Gao, D.Y. Yan, Hyperbranched polymers: from synthesis to applications, Prog. Polym. Sci. 29 (2004) 183–275.

[26] Z.J. Chen, L. Zhou, F.A. Zhang, C.B. Yu, Z.B. Wei, Multicarboxylic hyperbranched polyglycerol modified SBA-15 for the adsorption of cationic dyes and copper ions from aqueous media, Appl. Surf. Sci. 258 (2012) 5291–5298.

[27] Y. Fan, H.J. Liu, Y. Zhang, Yu. Chen, Adsorption of anionic MO or cationic MB from MO/MB mixture using polyacrylonitrile fiber hydrothermally treated with hyperbranched polyethylenimine, J. Hazard. Mater. 283 (2015) 321–328.

[28] H. Yoo, S.Y. Kwak, Surface functionalization of PTFE membranes with hyperbranched poly(amidoamine) for the removal of Cu^{2+} ions from aqueous solution, J. Membr. Sci. 448 (2013) 125–134.

[29] B. Yu, X.S. Jiang, G.L. Yin, J. Yin, Multistimuli-responsive hyperbranched poly (ether amine)s, J. Polym. Sci. Polym. Chem. 48 (2010) 4252–4261.

[30] W.S. Hummers, R.E. Offeman, Preparation of graphitic oxide, J. Am. Chem. Soc. 80 (1958) 1339.

[31] G.X. Zhao, J.X. Li, X.M. Ren, C.L. Chen, X.K. Wang, Few-layered graphene oxide nanosheets as superior sorbents for heavy metal ion pollution management, Environ. Sci. Technol. 45 (2011) 10454–10462.

[32] X.S. Liu, J.M. Cao, H. Li, J.Y. Li, Q. Jin, K.F. Ren, J. Ji, Mussel-inspired polydopamine: a biocompatible and ultrastable coating for nanoparticles in vivo, ACS Nano 7 (2013) 9384–9395.

[33] G. Moussavi, B. Barikbin, Biosorption of chromium(VI) from industrial wastewater onto pistachio hull waste biomass, Chem. Eng. J. 162 (2010) 893–900.

[34] C. Tian, H. Pei, W. Hu, J. Xie, Variation of cyanobacteria with different environmental conditions in Nansi Lake, China, J. Environ. Sci. 24 (2012) 1394–1402.

[35] Y.S. Ho, Effect of pH on lead removal from water using tree fern as the sorbent, Bioresour. Technol. 96 (2005) 1292–1296.

[36] L. Sun, H. Yu, B. Fugetsu, Graphene oxide adsorption enhanced by in situ reduction with sodium hydrosulfite to remove acridine orange from aqueous solution, J. Hazard. Mater. 203 (2012) 101–110.

[37] M. Srinivasan, C. Ferraris, T. White, Cadmium and lead ion capture with three dimensionally ordered macroporous hydroxyapatite, Environ. Sci. Technol. 40 (2006) 7054–7059.

[38] V.K. Gupta, M. Gupta, S. Sharma, Process development for the removal of lead and chromium from aqueous solutions using red mud–an aluminium industry waste, Water Res. 35 (2001) 1125–1134.

[39] L. Zhou, J. Jin, Z. Liu, X. Liang, C. Shang, Adsorption of acid dyes from aqueous solutions by the ethylenediamine-modified magnetic chitosan nanoparticles, J. Hazard. Mater. 185 (2011) 1045–1052.

[40] H. Wang, Y.F. Yu, Q.W. Chen, K. Cheng, Carboxyl-functionalized nanoparticles with magnetic core and mesopore carbon shell as adsorbents for the removal of heavy metal ions from aqueous solution, Dalton Trans. 40 (2010) 559–563.

[41] H. Zhang, H. Selim, Kinetics of arsenate adsorption–desorption in soils, Environ. Sci. Technol. 39 (2005) 6101–6108.

[42] R. Kumar, M. Barakat, Y. Daza, H. Woodcock, J. Kuhn, EDTA functionalized silica for removal of Cu(II), Zn(II) and Ni(II) from aqueous solution, J. Colloid Interface Sci. 408 (2013) 200–205.

[43] E. Repo, J.K. Warchoł, A. Bhatnagar, M. Sillanp, Heavy metals adsorption by novel EDTA-modified chitosan–silica hybrid materials, J. Colloid Interface Sci. 358 (2011) 261–267.

[44] Y.S. Ho, Review of second-order models for adsorption systems, J. Hazard. Mater. 136 (2006) 681–689.

[45] C. Ng, J.N. Losso, W.E. Marshall, R.M. Rao, Freundlich adsorption isotherms of agricultural by-product-based powdered activated carbons in a geosminwater system, Bioresour. Technol. 85 (2002) 131–135.

[46] X.X. Dong, Q. Wei, J. Yang, L.G. Yan, R. Feng, Highly efficient removal of heavy metal ions by amine-functionalized mesoporous Fe3O4 nanoparticles, Chem. Eng. J. 184 (2012) 132–140.

[47] Z.G. Jia, Q.Z. Wang, D.P. Ren, R.S. Zhu, Fabrication of one-dimensional mesoporous Fe_2O_3 nanostructure via self-sacrificial template and its enhanced Cr(VI) adsorption capacity, Appl. Surf. Sci. 264 (2013) 255–260.

[48] H. Wang, X.Z. Yuan, Y. Wu, H.J. Huang, Adsorption characteristics and behaviors of graphene oxide for Zn(II) removal from aqueous solution, Appl. Surf. Sci. 279 (2013) 432–440.

[49] S. Erenturk, E. Malkoc, Removal of lead(II) by adsorption onto Viscum album L.: effect of temperature and equilibrium isotherm analyses, Appl. Surf. Sci. 253 (2007) 4727–4733.

[50] L. Wang, J. Zhang, A. Wang, Fast removal of methylene blue from aqueous solution by adsorption onto chitosan-g-poly (acrylic acid)/attapulgite composite, Desalination 266 (2011) 33–39.

[51] E. Malkoc, Ni (II) removal from aqueous solutions using cone biomass of Thuja orientalis, J. Hazard. Mater. 137 (2006) 899–908.

[52] J.H. Chen, H.T. Xing, H.X. Guo, G.P. Li, W. Weng, S.R. Hu, Preparation, characterization and adsorption properties of a novel 3-aminopropyltriethoxysilane functionalized sodium alginate porous membrane adsorbent for Cr(III) ions, J. Hazard. Mater. 248 (2013) 285–294.

[53] K. Zargoosh, H. Abedini, A. Abdolmaleki, M.R. Molavian, Effective removal of heavy metal ions from industrial wastes using thiosalicylhydrazide-modified magnetic nanoparticles, Ind. Eng. Chem. Res. 52 (2013) 14944–14954.

[54] G.Z. Kyzas, M. Kostoglou, N.K. Lazaridis, Copper and chromium(VI) removal by chitosan derivatives-equilibrium and kinetic studies, Chem. Eng. J. 152 (2009) 440–448.

[55] G.Z. Kyzas, P.I. Siafaka, E.G. Pavlidou, K.J. Chrissafis, D.N. Bikiaris, Synthesis and adsorption application of succinyl-grafted chitosan for the simultaneous removal of zinc and cationic dye from binary hazardous mixtures, Chem. Eng. J. 259 (2015) 438–448.

[56] D.Y. Tang, Z. Zheng, K. Lin, J.F. Luan, J.B. Zhang, Adsorption of p-nitrophenol from aqueous solutions onto activated carbon fiber, J. Hazard. Mater. 143 (2007) 49–56.

[57] M.F.R. Pereira, S.F. Soares, J.J.M. Orfao, J.L. Figueiredo, Adsorption of dyes on activated carbons- influence of surface chemical groups, Carbon 41 (2003) 811–821.

[58] R. Arasteh, M. Masoumi, A.M. Rashidi, L. Moradi, V. Samimi, S.T. Mostafavi, Adsorption of 2-nitrophenol by multi-wall carbon nanotubes from aqueous solutions, Appl. Surf. Sci. 256 (2010) 4447–4455.

[59] P. Bradder, S.K. Ling, S. Wang, S. Liu, Dye adsorption on layered graphite oxide, J. Chem. Eng. Data 56 (2011) 138–141.

[60] L.H. Ai, C.Z. Zhang, F. Liao, Y. Wang, M. Li, L.Y. Meng, J. Jiang, Removal of methylene blue from aqueous solution with magnetite loaded multi-wall carbon nanotube: kinetic, isotherm and mechanism analysis, J. Hazard. Mater. 198 (2011) 282–290.

[61] L. Xiong, Y. Yang, J.X. Mai, W.L. Sun, C.Y. Zhang, D.P. Wei, Q. Chen, J.R. Ni, Adsorption behavior of methylene blue onto titanate nanotubes, Chem. Eng. J. 156 (2010) 313–320.

[62] I.E.M. Carpio, J.D. Mangadlao, H.N. Nguyen, R.C. Advincul, D.F. Rodrigues, Graphene oxide functionalized with ethylenediamine triacetic acid for heavy metal adsorption and anti-microbial applications, Carbon 77 (2014) 289–301.

[63] L.M. Cui, Y.G. Wang, L. Gao, L.H. Hu, L.G. Yan, Q. Wei, Bin Du, EDTA functionalized magnetic graphene oxide for removal of Pb(II), Hg(II) and Cu (II) in water treatment: adsorption mechanism and separation property, Chem. Eng. J. 281 (2015) 1–10.

[64] H.V. Tran, L.D. Tran, T.N. Nguyen, Preparation of chitosan/magnetite composite beads and their application for removal of Pb(II) and Ni(II) from aqueous solution, Mater. Sci. Eng. C 30 (2010) 304–310.

[65] D. Chauhan, N. Sankararamakrishnan, Highly enhanced adsorption for decontamination of lead ions from battery wastewaters using chitosan functionalized with xanthate, Bioresour. Technol. 99 (2008) 9021–9024.

[66] L.L. Fan, C.N. Luo, X.J. Li, F.G. Lu, H.M. Qiu, M. Sun, Fabrication of novel magnetic chitosan grafted with graphene oxide to enhance adsorption properties for methyl blue, J. Hazard. Mater. 215–216 (2012) 272–279.

[67] F. Liu, S. Chung, G. Oh, T.S. Seo, Three-dimensional grapheme oxide nanostructure for fast and efficient water-soluble dye removal, ACS Appl. Mater. Interfaces 4 (2012) 922–927.

[68] T.H. Liu, Y.H. Li, Q.J. Du, J.K. Sun, Y.Q. Jiao, G.M. Yang, Z.H. Wang, Y.Z. Xia, W. Zhang, K.L. Wang, H.W. Zhu, D.H. Wu, Adsorption of methylene blue from aqueous solution by graphene, Colloids Surf. B 90 (2012) 197–203